

# CrystEngComm

Accepted Manuscript



This is an *Accepted Manuscript*, which has been through the Royal Society of Chemistry peer review process and has been accepted for publication.

*Accepted Manuscripts* are published online shortly after acceptance, before technical editing, formatting and proof reading. Using this free service, authors can make their results available to the community, in citable form, before we publish the edited article. We will replace this *Accepted Manuscript* with the edited and formatted *Advance Article* as soon as it is available.

You can find more information about *Accepted Manuscripts* in the [Information for Authors](#).

Please note that technical editing may introduce minor changes to the text and/or graphics, which may alter content. The journal's standard [Terms & Conditions](#) and the [Ethical guidelines](#) still apply. In no event shall the Royal Society of Chemistry be held responsible for any errors or omissions in this *Accepted Manuscript* or any consequences arising from the use of any information it contains.

Cite this: DOI: 10.1039/c0xx00000x

www.rsc.org/xxxxxx

ARTICLE TYPE

## Nanostructured individual nacre tablet: A subtle designed organic-inorganic composite

Sheng-Nan Wang,<sup>a</sup> Xin-Qiao Zhu,<sup>a</sup> Xiao-Hui Yan,<sup>b</sup> Jing-Fei Deng,<sup>a</sup> Rizhi Wang<sup>c</sup> and Xiao-Xiang Wang\*<sup>a</sup>

Received (in XXX, XXX) Xth XXXXXXXXX 20XX, Accepted Xth XXXXXXXXX 20XX

DOI: 10.1039/b000000x

As natural evolution, nacre, a biogenic organic-inorganic composite, fulfills an ingenious combination of remarkable strength and toughness. Its basic building block, the individual nacre tablet, assumes an important mechanical function. Unravelling its design strategies can hence provide essential instruction for the pursuit of high-performance artificial composites. Here, nanostructure inside the individual nacre tablet (*Pinctada maxima*) was investigated using transmission electron microscopy techniques. Results show that organic matter is trapped inside the tablet in islet-like and sheet-like manner, respectively. More interestingly, crystal structure of aragonite scaffold is still continuous and homodromous throughout the whole tablet even in this case. A biomineralization mechanism of the tablet is discussed based on this finding.

### 15 Introduction

In order to survive in surrounding environment, mollusks evolved various elaborate shells to avoid fierce impact from predators. In general, they are of unique architecture, and hence gain superior mechanical performance. Nacre, inner iridescent layer of mollusk shells, has been taken as a research model for its regular structure and prominent mechanical behaviors. With addition of 5% organic matter, this natural organic-inorganic composite presents a precisely designed brick-and-mortar architecture and fulfills an ingenious combination of remarkable strength and toughness<sup>1-4</sup>. It inspires numerous researches to unravel its design strategies in pursuit of high-performance artificial composites<sup>5-11</sup>.

To create artificial nacre-like composites, designing the tablet-like inorganic building blocks with appropriate mechanical properties is indispensable<sup>12-15</sup>. Mechanical experiments demonstrate that nacre usually fractures in a tablet-pull-out mode, in which the organic matrix yields prior to the occurrence of tablet fracture<sup>4, 16-22</sup>. In this regard, the individual nacre tablet as the basic structural unit, must be strong and tough, which, actually, has been confirmed. Plastic deformation of the tablet was observed in nanoindentation tests<sup>23-25</sup> and the toughening origin was ascribed to its sophisticated nanostructure inside<sup>26-28</sup>. In view of this, revealing the nanostructure of the individual nacre tablet systematically has important guiding significance to design brick-like elementary unit with appropriate mechanical performance, which undoubtedly holds the key to mimic the artificial nacre-like composites.

The individual nacre tablet has long been regarded as a conventional single crystal for its single-crystal electron diffraction patterns. However, further investigations indicated that the tablet contains intracrystalline organics and has nanostructure<sup>23, 28-39</sup>. Recently, transmission electron microscopy

(TEM) and atomic force microscopy (AFM) investigations revealed that the individual nacre tablet is not a single crystal but rather composed of highly oriented nanocrystals or nanotables<sup>23, 28-33</sup> which are separated by the continuous organic framework<sup>23, 28-33</sup>. On the other hand, the isolate voids and strips were observed inside the individual nacre tablet, energy dispersive X-ray spectroscopy (EDX) and electron energy loss spectroscopy (EELS) investigations suggested that they should be the trapped intracrystalline organics<sup>34-36, 38, 39</sup>. Apparently, the sophisticated nanostructure of the tablet still remains bewildering, especially how the organic molecules are associated with the mineral host. Therefore, more systematic work is needed.

In this work, individual nacre tablet from shell of *Pinctada maxima* was investigated. Our results show that the islet-like and sheet-like organics are trapped in the continuous crystalline scaffold. The tablet's sophisticated nanostructure may endow itself with increased toughness, which could further contribute to the macroscopic fracture resistance of the shell.

### 65 Experimental

#### Materials:

Mature nacre materials from *Pinctada maxima* that belong to the class of bivalve were chosen for the investigation. Fresh shells were obtained from South China Sea. To minimize the detrimental effect of drying on the nanostructure and fracture behavior of the nacre tablet, the shells were cleaned and air delivered in ice to the laboratory. The block nacre samples were cut from the nacreous layer of the shells with a water-cooled, low-speed diamond saw.

#### 75 Scanning electron microscopy:

Block nacre samples were fractured by flexural tests carried out

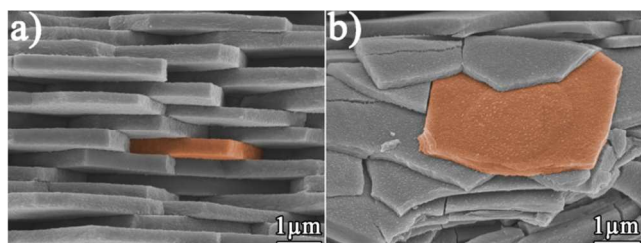


**Fig. 1** SEM image of the fractured nacre tablet. (a) Cross-section. (b) Top-surface. The individual nacre tablet is indicated by stain.

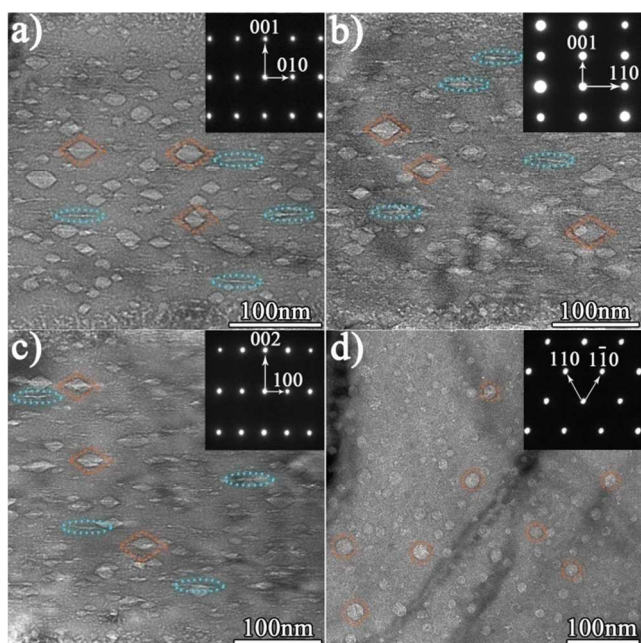


**Fig. 2** TEM bright-field images of the tablet at different zones. (a)-(c) Cross-section, dashed rhombus and ovals indicate the locations of quadrilateral and striation defects, respectively. (d) Top-surface, dashed circles indicate the locations of circular defect.

in a SANS CMT4203 universal testing machine. Then the samples were gold sputter coated and observed with HITACHI S-4800 field emission scanning electron microscopy at 5kV accelerating voltage.

#### Transmission electron microscope:

For nanostructure analysis, the block nacre were further cut into thin slices in thickness of 0.3mm by using a water-cooled, low-speed diamond saw. After mechanically grounding to 50 $\mu$ m in thickness and polishing in both sides, these thin slices were glued on the single-hole microscopy Cu-grids. Final thickness for electron transparency was performed with ion milling on precision ion polishing system (PIPS, Model 695, Gatan) equipped with a liquid nitrogen cooling controller. To minimize the detrimental cumulative effect of ion beam during the thinning process, the milling temperature was kept at -50 $^{\circ}$ C constantly. After perforation, the specimens were evaporated with a thin gold-coating layer to insure the evacuation of electrical charges during TEM operation. TEM observations were conducted with Tecnai G<sup>2</sup> F20 field emission transmission electron microscope at an accelerating voltage of 200kV.

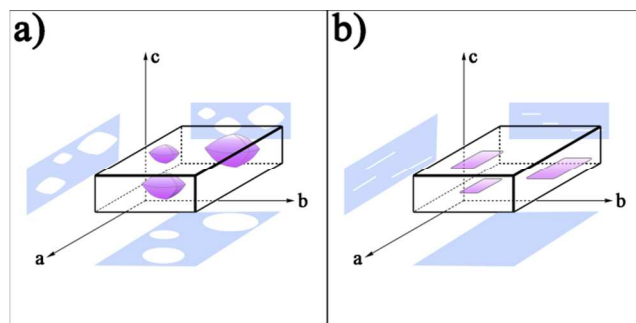


**Fig. 3** (a) Schematic illustration of a thin foil with islet-like defects incorporated, showing characteristics of quadrilaterals on the (hk0) planes and circles on the (001) plane. (b) Schematic illustration of a thin foil with sheet-like defects incorporated, showing characteristics of striations on the (hk0) planes while none contrast on the (001) plane.

## Results and discussion

Scanning electron microscopy (SEM) image of the fractured sample reveals highly ordered nacre tablets. The individual nacre tablet is approximately 300-400 nm in thickness and several micrometres in width (Figure 1).

To further investigate sophisticated nanostructure inside the individual nacre tablet, systematic TEM analyses were carried out. Figure 2 shows the magnified images of the tablet. The selected area electron diffraction (SAED) pattern insets exhibit characteristics of single crystal that can be indexed as the [100] (Figure 2a), [010] (Figure 2b), [110] (Figure 2c) and [001] (Figure 2d) zone axes of the aragonite crystal, respectively (lattice parameters  $a = 4.9623 \text{ \AA}$ ,  $b = 7.968 \text{ \AA}$ ,  $c = 5.7439 \text{ \AA}$ , space group Pmcn (62), JCPDS file 41-1475). In cross-sections of the tablet (Figure 2a-2c), trapped quadrilateral and striation defects (indicated with dashed rhombus and ovals, respectively) are observed. The quadrilateral defects range from 10-40 nm in size, and the striation defects are approximately 20-60 nm in length and 1-2 nm in thickness. While, on the (001) crystal plane (top-surface) of the tablet (Figure 2d), only circular defects (indicated with dashed circles) in size of 10-40 nm can be identified. Tens of tablets were surveyed in the present study and they showed coincident morphology when viewed down the same orientation.

The intracrystalline defects have attracted increasing attention in recent years. Lots of efforts have been laid on their three-dimensional distribution<sup>34, 36, 38, 40</sup>. Electron tomography reconstructions, combined with TEM, exposed that quadrilateral defects are randomly distributed inside the individual nacre tablet. The shape of these defects was reconstructed to be islet-like in three-dimensional space<sup>34, 38</sup>. As seen in Figure 3a, a thin foil with islet-like defects incorporated exhibits characteristics of quadrilaterals and circles in projections of the [hk0] zone axes and the [001] zone axis, respectively, coinciding with the morphology observed by TEM (Figure 2). In contrast, because of the limited resolution of the tomography data<sup>34</sup>, the striation defects with a thickness of 1-2 nm were not clearly identified. This kind of defects has been discovered in previous study on the nacre of *Hyriopsis cumingii*<sup>35</sup>. Interestingly, they did not show any contrast either in the diffraction contrast or the Z-contrast operation when viewed down the [001] zone axis, as a result, they

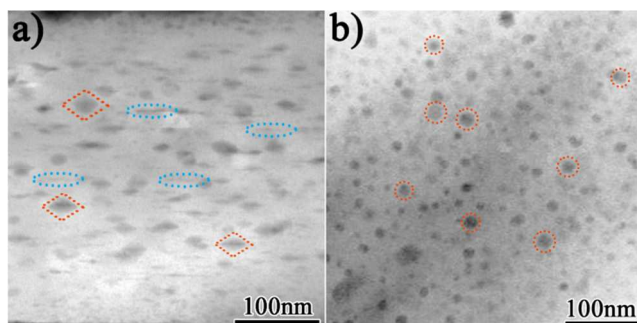


**Fig. 4** HAADF-STEM images of the tablet. (a) Cross-section. (b) Top-surface. The defects (indicated by dashed rhombus, ovals and circles) show darker contrast compared to the aragonite scaffold.

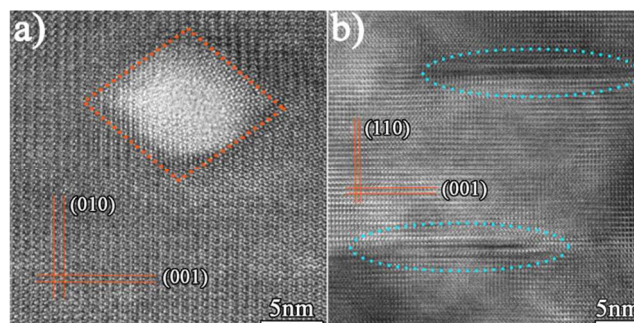


**Fig. 6** Enlarged HRTEM images of the areas containing organics. (a) The islet-like organics (indicated with a dashed rhombus) trapped in the homodromous aragonite lattice sequences. (b) The sheet-like organics (indicated with dashed ovals) lie on the (001) plane of the continuous aragonite crystal.

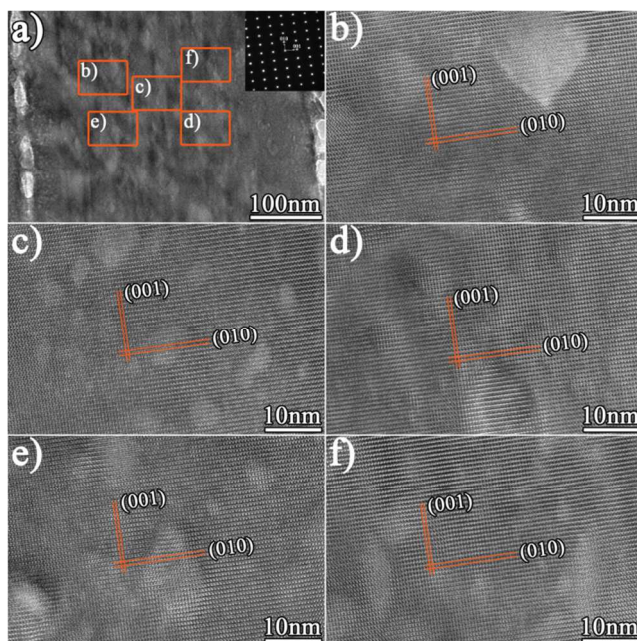


**Fig. 5** (a) Bright-field image of an individual nacre tablet. The corresponding SAED pattern inset is indexed as the [100] zone of aragonite crystal. (b)-(f) HRTEM images taken from the rectangular areas labelled in (a), showing continuous and homodromous aragonite lattice sequences.

were suggested to be thin sheet-like in three-dimensional space<sup>39</sup>. To make more detailed analysis geometrically here, a schematic diagram of thin foil with sheet-like defects is indicated in Figure 3b. The corresponding projections of the [hk0] zone axes exhibit characteristics of striations. While, when viewed down the [001] zone, as the thickness of the sheet-like defects (1-2 nm) is much smaller than the foil (50-100 nm), these defects could not display any contrast on the (001) plane, as a result, only circular defects can be observed.

Next, there comes another question - what exactly these defects are? To unlock this mystery, high-angle annular dark-field scanning transmission electron microscopy (HAADF-STEM) imaging measurements were performed. In this technique, electrons scattered at large angles are detected, as a result, those areas of the specimen that contain lighter atoms appear darker; the areas containing heavier atoms appear brighter. As shown in HAADF-STEM images (Figure 4), darker defects are embedded within brighter aragonite scaffold, implying that

these defects should be either voids or intracrystalline organics. Previous researches demonstrated that these defects contain an increased amount of carbon<sup>34, 36, 38, 40</sup>, which was further supported by our EDX analysis (Figure S1). Taken together, these results indicate that rather than voids, the islet-like and sheet-like defects should be the locations of intracrystalline organics. Their existence was speculated to increase the crack propagation path and thus enhance the fracture resistance of the tablet<sup>34, 38</sup>.

Whereas the previous researches laid more emphasis on the 3D distribution of the intracrystalline organics, the existing mode of the mineral phase still remains open. To gain more information here, detailed high resolution transmission electron microscopy (HRTEM) analyses were conducted. As shown in Figure 5, HRTEM images from different areas of a tablet exhibit regular and continuous aragonite lattice sequences. These homodromous lattice sequences, extending to a wide range in tablet, show no tendency to rotate or distort. Significantly, no grain boundaries or any transition areas are observed. To further explore how the organics are accommodated by aragonite scaffold, the HRTEM images for areas containing the organics are obtained. The islet-like organics (indicated with dashed rhombus), showing none crystal lattice in centre, are trapped in homodromous aragonite scaffold (Figure 6a). Similarly, the sheet-like organics (indicated with dashed ovals), approaching 30 nm in length and 2 nm in thickness, lie on the (001) plane of the continuous aragonite crystal lattice (Figure 6b). Following these observations, it is most likely that the aragonite scaffold is homogeneous and continuous throughout the whole tablet, and the organics are trapped inside without disturbing the scaffold's integrity.

It has been long thought that the individual nacre tablet is a conventional single crystal for its single-crystal electron diffraction patterns. In recent years, with the discoveries of the organics and nanostructures inside the tablet, pseudo-single-crystal, composed of co-oriented nanocrystals separated by the continuous organic framework, was considered as the nature of the tablet<sup>28-31, 33</sup>. However, these nanocrystals were not observed in our present study. The aragonite host shows extremely consistent contrast throughout the whole tablet both in diffraction contrast, HAADF-STEM operation and HRTEM. Given its single-crystal diffraction patterns, it seems remarkable that rather than a pseudo-single-crystal, the tablet is a veritable single

crystal.

To reveal whether the present nanostructure is the substantive characteristics of the tablet or the artifacts of sample preparation, a geological aragonite sample was prepared by using the same method. Compared with nacre tablets, the geological aragonite shows uniform contrast in a wide area, no intracrystalline inclusions were observed (Figure S2). In view of this, the nanostructure presented in our study should be the intrinsic property of the tablet.

Apart from the damage caused by sample preparation process, the effect of the the electron beam during TEM observations should also be considered. As we know, the aragonite crystal, the inorganic phase of the nacre tablets, is a metastable phase of the calcium carbonate, which could be easily damaged by high-velocity motional electrons (acceleration voltage is 200kV). Our in situ irradiation experiments demonstrate that exposure to the electron beam at high magnification for seconds can transform the tablet into polycrystal, leading to the destruction of its single crystal characteristics (Figure S3). In this context, the nanograin structure observed in previous TEM investigations<sup>30,33,41</sup> can be reasonably explained.

On considering the beam-sensibility of this biogenic material, the electron optical parameters used for SAED and HRTEM imaging have been carefully chosen during this experiment. A smaller condenser diaphragm and larger spot size have been employed to decrease the electron irradiation damage as much as possible. Compared to a larger dose value which would cause the severe irradiation damage, these selected electron optical parameters are benefit to reflect intrinsic structural information during the imaging procedure. To exhibit the electron optical parameter change, two operation modes were compared (Table S1). Consequently, in order to get a veritable HRTEM image, the beam current should be kept in an extraordinary low value, meanwhile, the exposure and photograph time should be controlled, either.

The large block (110) twins have been observed in nacre of *Pinctada maxima* in previous study<sup>39</sup>. Different from the nanotwins generally observed in mollusk shells<sup>42,43</sup>, the large block twins exhibit a straight twinning plane propagating across the whole tablet. Based on this observation, atom-by-atom attachment was used to explain the formation mechanism of these block twins by referring to the classical recrystallization model. On the other hand, considering the nanoparticle morphology observed inside the tablet<sup>23,28</sup>, the non-classical particle-mediated crystallization pathway seems also reasonable. Based on the oriented attachment mechanism, this growth process is prone to result in the formation of a mesocrystal composed by co-oriented nanocrystals<sup>44</sup>. In this case, structural defects such as dislocations, stacking faults and grain boundaries should be inescapable, and the straight twinning plane propagating across the whole tablet might hardly form. As a result, the oriented attachment mechanism is inadequate to form a veritable single crystal. Recently, the oriented attachment and Ostwald ripening mechanism were proposed to occur simultaneously<sup>45</sup>, which might offer a reasonable explanation of our experiment results. The process can be summarized as follows: In the early stages of mineralization, oriented attachment mechanism may occur

predominantly. With an extended ineralization time, Ostwald ripening mechanism, to some extent, plays an important role to assist the oriented attachment process to from a veritable single crystal<sup>46</sup>. Yet, given that the detailed mineralization process of the tablet is still open, further work is necessary.

## Conclusions

In summary, the nanostructure inside the individual nacre tablet of *Pinctada maxima* was investigated by TEM. Results show that the aragonite scaffold is homogeneous and continuous throughout the whole tablet, and the islet-like and sheet-like organics are trapped inside without disturbing the scaffold's integrality. This precisely designed nanostructure may be beneficial to reveal the origin of the tablet's eminent fracture behavior and further provide design strategies for artificial nacre-like composites.

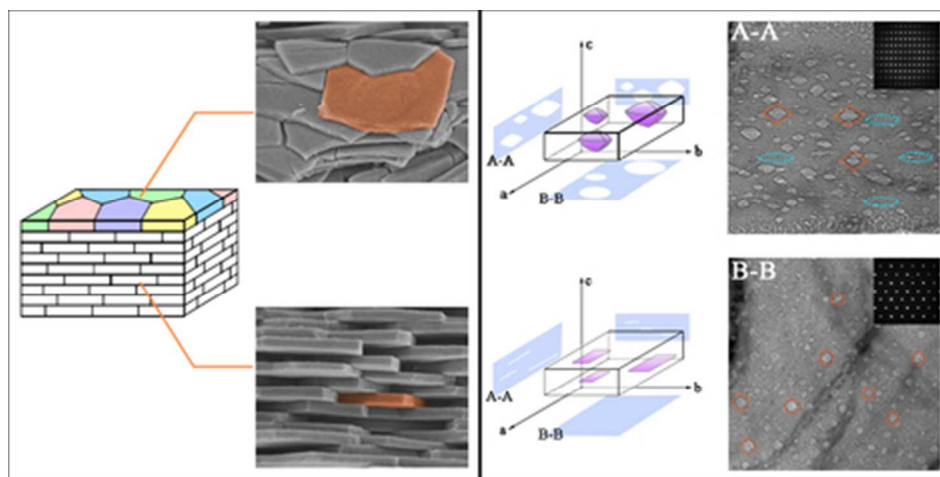
## Acknowledgements

We acknowledge Da-Hui Yu from South China Sea Fisheries Research Institute for providing us with *Pinctada maxima* shells. We also appreciate Chuan-Hong Jin and Yue-Wu Zeng from Center of Electron Microscope, Zhejiang University, for TEM technical support.

## References

- <sup>a</sup> Department of Materials Science and Engineering, Zhejiang University, Hangzhou 310027, China. Fax: +86 571 87952255; Tel: +86 0571 87952255; E-mail: [msewangxx@zju.edu.cn](mailto:msewangxx@zju.edu.cn)
- <sup>b</sup> Department of Mechanical and Automation Engineering, The Chinese University of Hong Kong, Shatin, N.T., Hong Kong, China. E-mail: [shyan@mae.cuhk.edu.hk](mailto:shyan@mae.cuhk.edu.hk)
- <sup>c</sup> Department of Materials Engineering, University of British Columbia, Vancouver, BC V6T 1Z4, Canada. E-mail: [rzwang@interchange.ubc.ca](mailto:rzwang@interchange.ubc.ca)
- <sup>†</sup> Electronic Supplementary Information (ESI) available: Fig. S1–S3 as mentioned in the text. See DOI: 10.1039/b000000x/
1. J. D. Currey, Proceedings of the Royal Society B: Biological Sciences, 1977, **196**, 443-463.
2. A. P. Jackson, J. F. V. Vincent and R. M. Turner, Proceedings of the Royal Society B: Biological Sciences, 1988, **234**, 415-440.
3. R. Menig, M. H. Meyers, M. A. Meyers and K. S. Vecchio, Acta Materialia, 2000, **48**, 2383-2398.
4. F. Barthelat, H. Tang, P. Zavattieri, C. Li and H. Espinosa, Journal of the Mechanics and Physics of Solids, 2007, **55**, 306-337.
5. Z. Y. Tang, N. A. Kotov, S. Magonov and B. Ozturk, Nature materials, 2003, **2**, 413-U418.
6. P. Podsiadlo, A. K. Kaushik, E. M. Arruda, A. M. Waas, B. S. Shim, J. Xu, H. Nandivada, B. G. Pumplun, J. Lahann, A. Ramamoorthy and N. A. Kotov, Science, 2007, **318**, 80-83.
7. E. Munch, M. E. Launey, D. H. Alsem, E. Saiz, A. P. Tomsia and R. O. Ritchie, Science, 2008, **322**, 1516-1520.
8. Y.-Q. Li, T. Yu, T.-Y. Yang, L.-X. Zheng and K. Liao, Advanced Materials, 2012, **24**, 3426-3431.
9. Q. Cheng, M. Li, L. Jiang and Z. Tang, Advanced Materials, 2012, **24**, 1838-1843.
10. X. Q. Li and H. C. Zeng, Adv Mater, 2012, **24**, 6277-6282.
11. W. Cui, M. Li, J. Liu, B. Wang, C. Zhang, L. Jiang and Q. Cheng, ACS nano, 2014, **8**, 9511-9517.
12. L. J. Bonderer, A. R. Studart and L. J. Gauckler, Science, 2008, **319**, 1069-1073.
13. J. Wang, Q. Cheng and Z. Tang, Chemical Society Reviews, 2012, **41**, 1111-1129.
14. F. Bouville, E. Maire, S. Meille, B. Van de Moortele, A. J. Stevenson and S. Deville, Nature materials, 2014, **13**, 508-514.
15. Q. Cheng, L. Jiang and Z. Tang, Accounts of Chemical Research, 2014, **47**, 1256-1266.

16. R. Z. Wang, Z. Suo, A. G. Evans, N. Yao and I. A. Aksay, *Journal of Materials Research*, 2001, **16**, 2485-2493.
17. A. G. Evans, Z. Suo, R. Z. Wang, I. A. Aksay, M. Y. He and J. W. Hutchinson, *Journal of Materials Research*, 2001, **16**, 2475-2484.
- 5 18. F. Barthelat and H. D. Espinosa, *Experimental Mechanics*, 2007, **47**, 311-324.
19. A. Y. Lin and M. A. Meyers, *Journal of the mechanical behavior of biomedical materials*, 2009, **2**, 607-612.
20. H. D. Espinosa, A. L. Juster, F. J. Latourte, O. Y. Loh, D. Gregoire and P. D. Zavattieri, *Nature communications*, 2011, **2**, 173.
- 10 21. H. Kakisawa and T. Sumitomo, *Science and Technology of Advanced Materials*, 2011, **12**, 064710.
22. R. Wang and H. S. Gupta, *Annual Review of Materials Research*, 2011, **41**, 41-73.
- 15 23. X. Li, W.-C. Chang, Y. J. Chao, R. Wang and M. Chang, *Nano Letters*, 2004, **4**, 613-617.
24. B. J. F. Bruet, H. J. Qi, M. C. Boyce, R. Panas, K. Tai, L. Frick and C. Ortiz, *Journal of Materials Research*, 2005, **20**, 2400-2419.
25. X. Li, *Jom*, 2007, **59**, 71-74.
- 20 26. T. Sumitomo, H. Kakisawa, Y. Owaki and Y. Kagawa, *Journal of Materials Research*, 2008, **23**, 3213-3221.
27. Z. Huang and X. Li, *Scientific reports*, 2013, **3**, 1693.
28. X. Li, Z.-H. Xu and R. Wang, *Nano Letters*, 2006, **6**, 2301-2304.
29. K. Takahashi, H. Yamamoto, A. Onoda, M. Doi, T. Inaba, M. Chiba, 25 A. Kobayashi, T. Taguchi, T. A. Okamura and N. Ueyama, *Chemical communications*, 2004, 996-997.
30. M. Rousseau, E. Lopez, P. Stempfle, M. Brendle, L. Franke, A. Guette, R. Naslain and X. Bourrat, *Biomaterials*, 2005, **26**, 6254-6262.
- 30 31. Y. Oaki and H. Imai, *Angewandte Chemie*, 2005, **44**, 6571-6575.
32. Y. Oaki, A. Kotachi, T. Miura and H. Imai, *Advanced Functional Materials*, 2006, **16**, 1633-1639.
33. X. Li and Z. Huang, *Physical Review Letters*, 2009, **102**, 075502
34. K. Gries, R. Kroger, C. Kubel, M. Fritz and A. Rosenauer, *Acta biomaterialia*, 2009, **5**, 3038-3044.
- 35 35. L. Xie, X. X. Wang and J. Li, *Journal of structural biology*, 2010, **169**, 89-94.
36. M. Suzuki, T. Okumura, H. Nagasawa and T. Kogure, *Journal of Crystal Growth*, 2011, **337**, 24-29.
- 40 37. X.-H. Yan, S.-N. Wang, X.-J. Zhang, X.-X. Wang and R. Wang, *CrystEngComm*, 2011, **13**, 7202.
38. S. Younis, Y. Kauffmann, L. Bloch and E. Zolotoyabko, *Crystal Growth & Design*, 2012, **12**, 4574-4579.
39. S.-N. Wang, X.-H. Yan, R. Wang, D.-H. Yu and X.-X. Wang, 45 *Journal of structural biology*, 2013, **183**, 404-411.
40. H. Li, H. L. Xin, M. E. Kunitake, E. C. Keene, D. A. Muller and L. A. Estroff, *Advanced Functional Materials*, 2011, **21**, 2028-2034.
41. F. Barthelat, C.-M. Li, C. Comi and H. D. Espinosa, *Journal of Materials Research*, 2006, **21**, 1977-1986.
- 50 42. M. Kudo, J. Kameda, K. Saruwatari, N. Ozaki, K. Okano, H. Nagasawa and T. Kogure, *Journal of structural biology*, 2010, **169**, 1-5.
43. H. Mukai, K. Saruwatari, H. Nagasawa and T. Kogure, *Journal of Crystal Growth*, 2010, **312**, 3014-3019.
- 55 44. T. Wang, H. Cölfen and M. Antonietti, *Journal of the American Chemical Society*, 2005, **127**, 3246-3247.
45. H. Zhan, X. Yang, C. Wang, C. Liang and M. Wu, *The Journal of Physical Chemistry C*, 2010, **114**, 14461-14466.
46. J. Fang, B. Ding and H. Gleiter, *Chemical Society Reviews*, 2011, 60 **40**, 5347-5360.



The individual nacre tablet from the shell of *Pinctada maxima* is an organic-inorganic single-crystal composite where the islet-like and sheet-like organics are trapped in the continuous crystalline scaffold.  
39x19mm (300 x 300 DPI)